

Reflection and transmission properties of a finite-length electron plasma grating

Cite as: Matter Radiat. Extremes 7, 054402 (2022); doi: 10.1063/5.0096386

Submitted: 18 April 2022 • Accepted: 10 July 2022 •

Published Online: 16 August 2022



View Online



Export Citation



CrossMark

G. Lehmann^{a)}  and K. H. Spatschek 

AFFILIATIONS

Institut für Theoretische Physik I, Heinrich-Heine-Universität Düsseldorf, D-40225 Düsseldorf, Germany

Note: This paper is a part of the Special Topic Collection on Plasma Optics.

^{a)} Author to whom correspondence should be addressed: goetz@tpl.uni-duesseldorf.de

ABSTRACT

Considered here is a plasma grating generated by two counterpropagating short laser pulses. Because of the shortness of the laser pulses, the plasma dynamics are determined by only electrons, which respond to the ponderomotive pressure generated by the interacting laser fields. An electron grating cannot exist for longer than the inverse ion plasma frequency, and so because of the limited time of the ponderomotive pressure, both the life time and spatial extent of an electron grating are finite. When one of the short laser pulses is circularly polarized (propagating in the x direction with electric field vectors in the yz plane) and the other is linearly y -polarized, the electron grating is produced by the y components. Meanwhile, the z component is partially reflected, and only a fraction of it is transmitted. Thus, the finite plasma grating can either alter the polarization of the yz -polarized pulse or act as a pulse splitter. The present paper is focused on the reflection and transmission rates. The action of the density grating on the z component cannot be explained by the Bloch wave theory for infinite crystals, and instead a theory is developed based on four-wave mixing, which explains the transmission and reflection of the z component when interacting with a grating of finite extent.

© 2022 Author(s). All article content, except where otherwise noted, is licensed under a Creative Commons Attribution (CC BY) license (<http://creativecommons.org/licenses/by/4.0/>). <https://doi.org/10.1063/5.0096386>

I. INTRODUCTION

Because the damage threshold of a plasma is orders of magnitude higher than that of solid-state optics, plasma components are investigated intensively for manipulating laser light at high intensities.^{1–3} In recent years, plasma mirrors,^{4,5} wave- and q-plates,^{6,7} and plasma-based polarizers^{8–10} have shown enormous potential as high-intensity photonic devices, and active consideration is being given to plasma optical modulators,¹¹ active plasma lenses,^{12–15} plasma holograms,^{16–19} terahertz radiation sources,²⁰ and plasma-based beam combiners for very high fluence and energy.²¹ Also, plasma parametric amplification^{22–27} and the use of plasma mirrors for focusing are now part of the newly developing domain of plasma optics, which will eventually lead to high-intensity lasers.²⁸

Among the proposed optical components are plasma gratings,^{29–31} also known as plasma photonic crystals (PPCs).^{32–35} A PPC can be understood as a periodic modulation of the refractive index, with a period close to the wavelength of light.³⁶ The formation of deep electron and ion density gratings by using two

counterpropagating and intersecting laser pulses began to be studied in the early 2000s,^{29,37} and since then many details and applications have been worked out.^{4,5,10,11,18,38–46} PPCs are now promising optical devices that can withstand laser intensities above the solid-state damage threshold, and many applications have been discussed.

To date, the main interest has been robust gratings that are established relatively slowly and persist on time scales longer than the inverse ion plasma frequency. However, for some problems in basic physics (e.g., frequency up-conversion of lasers and photon acceleration^{47–52}), it may be desirable to have a rapidly created and evolving plasma grating at one's disposal, and the main aim herein is to elucidate some features of such a rapid grating. Note that a rapid electron grating appears in the initial phase of a ponderomotive ion grating, but for the latter, the two generating counterpropagating pump laser pulses persist for sufficiently long times that ions may react. Instead, if one uses short pump pulses, then only the first electron reaction appears, and it will persist for as long as the pump pulses intersect each other. Therefore the following question arises: how can one study, for example, the reflection and transmission properties of such a volatile grating? The answer is related

to nonlinear polarization transfer and control of two laser beams overlapping in a uniform nonlinear medium.⁵³

We investigate the short-pulse interaction scenario in which a circularly polarized laser pulse interacts with a counterpropagating y -polarized laser pulse. We treat the circularly polarized wave as a superposition of two linearly polarized components that we designate as z - and y -polarized, respectively, and the interaction of the y components (parallel polarization) leads to standing density changes in the plasma. Because of the shortness of the laser beams, the plasma dynamics are dominated initially by only electrons as they respond to the ponderomotive pressure, and an electron grating can appear for a time of no more than the inverse ion plasma frequency, with the wave with a z component propagating in the grating. Note that a standing electron grating differs from the moving train of potential wells of two slightly detuned laser pulses that collide in a plasma and give rise to a short-duration burst of coherent terahertz radiation.⁵⁴

Because of the limited time of the ponderomotive pressure, an electron grating is finite in both space and time. Therefore, its properties cannot be explained by (infinite) Bloch wave analysis, and instead we develop a theory based on four-wave mixing,^{31,55–57} which explains the transmission and reflection of the z -polarized component when interacting with the grating. The present four-wave-mixing theory differs from previous models because we do not have parallel polarization of all four waves. This allows us to simplify the otherwise complex scenario into two manageable parts, i.e., (i) the generation of a grating by the y components and (ii) propagation of the z component in a modulated plasma, and we compare the predictions of the four-wave-mixing model with the results of extensive particle-in-cell (PIC) simulations. An alternative to the present modeling is analysis with a finite transfer-matrix calculation for layered matter, and that method is outlined in the Appendix (perhaps for later use when considering more details of grating structures); however, we do not evaluate the transfer-matrix method in all its specifics because the much simpler four-wave-mixing model already gives convincing results.

The rest of this paper is organized as follows. In Sec. II, we present the considered arrangement and PIC simulations. The simulations are for counterpropagating and interacting short laser pulses of the same frequency; by short, we mean that the duration of a laser pulse is of the order of 40 fs in a plasma whose density is 5% of the critical density. We analyze the generated electron grating itself and its transmission and reflection properties for electromagnetic waves. In Sec. III, we discuss the understanding provided by the PIC simulations, and we develop a four-wave-mixing theory to interpret the numerical results. We conclude in Sec. IV with a short summary and outlook, and in the Appendix we discuss an alternative method for analyzing finite PPCs.

II. PARTICLE-IN-CELL SIMULATION OF A FINITE ELECTRON GRATING

A. General arrangement

An electron grating appears when two counterpropagating laser pulses interact in a plasma, and the scenario is sketched in Fig. 1. Figure 1(a) shows the initial state. In general, the laser pulse propagating from the left can be either linearly or circularly

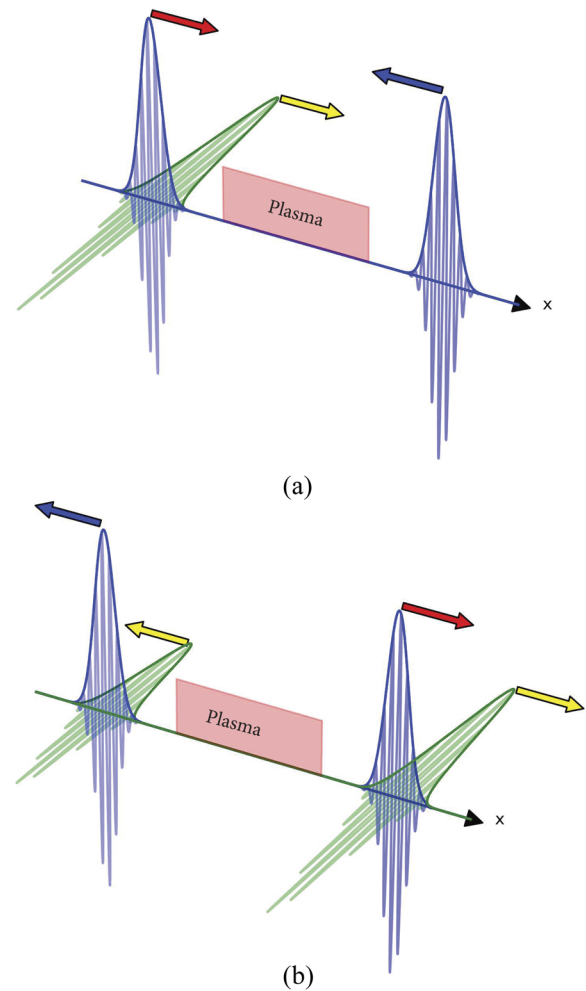


FIG. 1. (a) Initial situation in which two counterpropagating pulses approach a plasma slab; the left one (in purple and green) is circularly polarized, while the right one (in purple) is linearly polarized. (b) Transmission and reflection after the initial pulses have traversed the plasma.

polarized, and in the latter case we decompose it into two linearly polarized ones; the left beam propagates in the positive x direction and comprises a y -polarized component (in purple) and a z -polarized component (in green). The second laser beam (propagating from the right in the negative x direction) is always y -polarized (in purple). The y components produce the plasma grating, while the z component feels the density modulations. Figure 1(b) shows a later stage at which the original (initial) pulses have left the plasma, and we observe transmission and reflection; of particular interest here is the behavior of the z component (in green).

The two laser beams shown in Fig. 1(a) should be short, by which we mean that the duration of laser-pulse overlap is less than the inverse ion plasma frequency. Below, we present some typical numbers.

The vacuum laser frequency is $\omega_0 \approx 2.35 \times 10^{15} \text{ s}^{-1}$, leading to a period of $\tau_0 = \frac{2\pi}{\omega_0} \approx 2.6 \text{ fs}$. The wavelength is $\lambda_0 = 0.8 \mu\text{m}$, and the

wavenumber is $k_0 \approx 8 \times 10^4 \text{ cm}^{-1}$. We measure the mean (electron) plasma density in terms of the critical density n_c , with the latter being when the laser frequency equals the plasma frequency, i.e., $\omega_0 = \sqrt{4\pi n_c e^2 / m_e}$. When $n_0 = 0.05 n_c$, we obtain $\omega_{pe0} \approx 0.528 \times 10^{15} \text{ s}^{-1}$ and $\omega_{pe0}^{-1} \approx 1.9 \text{ fs}$. For a hydrogen plasma, the ion plasma frequency is $\omega_{pi} \approx 1.23 \times 10^{13} \text{ s}^{-1}$ and $\omega_{pi}^{-1} \approx 80 \text{ fs}$. We assume a typical pulse-duration FWHM (full width at half maximum of the electric field) as being 40 fs. The y components of the two laser beams may have equal intensities of order $I_0 = 5 \times 10^{16} \text{ W/cm}^2$, leading to a normalized vector potential $a_0 = eA_0/m_e c$ of the order of $a_0^2 \approx 2.3 \times 10^{-2}$.

In Sec. II C, we present PIC simulations showing the growth and lifetime of a pure electron grating.

B. Simulation technique and parameters

To simulate the interaction of the laser pulses in a one-dimensional geometry, we use the EPOCH particle-in-cell (PIC) code.⁵⁸ The total length of the simulation box is $400 \mu\text{m}$, and we use 15 000 cells (i.e., 30 cells per λ_0). In the center of the simulation box sits a (pre-ionized) hydrogen plasma slab of $100 \mu\text{m}$ in length with homogeneous density $n_0 = 0.05 n_c$. To the left and right of the plasma, there is $150 \mu\text{m}$ of vacuum. We simulate mobile electrons and ions ($Z = 1$, $m_i = 1836 m_e$) and use 250 pseudoparticles per species per occupied cell. We use the cold-plasma approximation, but we also performed several runs with finite electron temperature, and when varying the latter (e.g., around 100 eV) we found no significant changes.

From the left boundary of the simulation domain, we inject a circularly polarized laser pulse with electric field components E_y and E_z , and from the right boundary we inject a linearly polarized laser pulse of equal duration but with only an E_y component. The E_y components of the two pulses have equal intensity, and hereinafter mention of pulse intensity refers to that of the E_y components. The

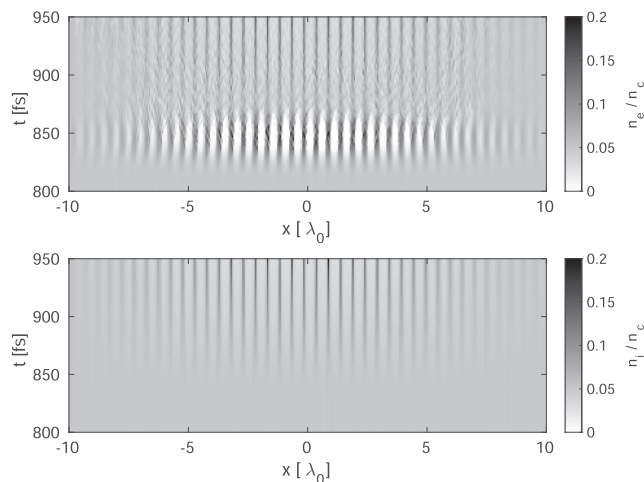


FIG. 2. Temporal evolutions of electron density n_e (upper) and ion density n_i (lower) in center of plasma. The initial homogeneous plasma density is $n_0 = 0.05 n_c$. At 830 fs, the laser pulses start interacting. Their duration is 40 fs (FWHM), and the E_y components have equal intensity of 10^{17} W/cm^2 .

E_z component of the circularly polarized pulse has the same intensity as that of the E_y component, otherwise the pulse would be elliptically polarized; however, the intensity of the E_z component could be less than that of the E_y component, and all subsequent conclusions would still be valid. We define the pulse duration τ as the FWHM of the electric field and use a Gaussian temporal pulse shape. The pulses arrive at the center of the simulation box (and thus of the plasma slab) at the same time.

C. Electron grating

Here, we present results for the density ripples produced by interacting laser pulses, and a typical example is shown in Fig. 2. We

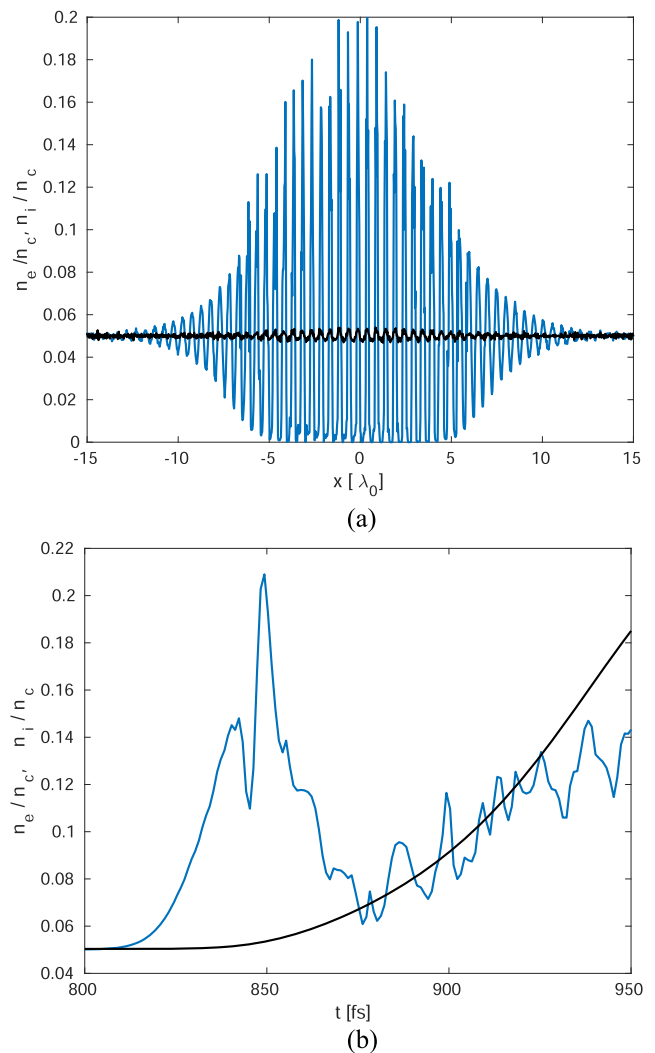


FIG. 3. (a) Spatial modulations of electron density (blue or light gray line) and ion density (black line) at $t = 850 \text{ fs}$. (b) Temporal evolutions of electron density (blue or light gray line) and ion density (black line) at $x = 0.5 \lambda_0$. The main overlap of the two laser pulses occurs between 830 and 870 fs, and the parameter values are the same as those for Fig. 2.

plot the temporal evolution of electron (upper figure) and ion (lower figure) density contours vs x , with the spatial coordinate in units of λ_0 and time t in femtoseconds.

Between 830 and 870 fs, the y -polarized components of the two 40 fs FWHM laser pulses with equal intensity of 10^{17} W/cm² overlap and drive a strong electron density modulation. During that time period, the ions are mostly quiet; their response sets in later and leads to the typical behavior of an ion grating.

Figure 3(a) shows a snapshot of the electron grating at time $t = 850$ fs for the same parameter values as those for Fig. 2. Clearly, the grating has a finite extent of over ~ 25 wavelengths λ_0 . The distribution of the density spikes is inhomogeneous, reflecting the pulse shapes of the driving laser pulses. Therefore, we cannot expect exact agreement (in all details) with analytical models based on finite but more-or-less rectangular density grating distributions. Note that the grating distribution is almost independent of the polarization of the left laser pulse if the y component in the circularly polarized case has the same amplitude as that in the linearly polarized case.

To demonstrate the different time scales on which electrons and ions react to the overlapping laser pulses, in Fig. 3(b) we show the electron and ion densities in the center of the grating as functions of time; this is where we observe the largest electron density modulation throughout the simulation. The electrons react almost instantaneously to the laser fields once the two driving pulses begin to overlap ($t \approx 810$ fs), and the modulation of the electron density then follows closely that of the local laser intensity. After $t \approx 850$ fs, the two pulses separate and the local electron density relaxes to almost its initial value. Meanwhile, the ions ($\omega_{pi}^{-1} \approx 80$ fs) have been attracted to the electron density spike and have begun their dynamics, which lead eventually to the formation of an electron-ion plasma grating. This collective grating forms on a time scale of $\mathcal{O}(\omega_{pi}^{-1})$ and has been studied previously; herein,

we focus on the electron grating that occurs on the time scale of $\mathcal{O}(\omega_{pe}^{-1})$.

D. Concurrent interaction of electromagnetic pulses

Here, we focus on the behavior of the E_z component when the left driving laser pulse is circularly polarized. Typical distributions of electric fields E_y and E_z are shown in Fig. 4 before (a) and after (b) interaction of the initial laser pulses.

Starting with the two pulses having equal amplitude before interacting [case (a) in Fig. 4], we recognize that after interaction [case (b) in Fig. 4] the field components E_y and E_z are being reflected and transmitted, respectively. For the y component, it is difficult to distinguish between reflection and transmission because we have two counterpropagating E_z fields already at the beginning. However, the two E_z pulses in the lower part of Fig. 4 can clearly be apportioned to reflection and transmission, respectively. In the absence of E_z , the two E_y pulses labeled with (b) (upper panel of Fig. 4) would be symmetric, and their slight asymmetry for $E_z \neq 0$ points to (nonlinear) interaction effects that are not considered further here.

In Sec. II E, we investigate how the transmission and reflection rates depend on the plasma and laser parameters.

E. Transmission and reflection

Transmission and reflection of the E_z field depend mainly on two parameters, i.e., (i) the FWHM pulse duration τ and (ii) the intensity of the laser pulses that drive the electron grating. From the simulations, we determine the fractions R and T of the incident pulse energy that is reflected and transmitted, respectively; for $R = 1$, the E_z field would be completely reflected, and for $T = 1$ it would be completely transmitted. We obtain these fractions by summing E_z^2 in the left and right vacuum regions before and after

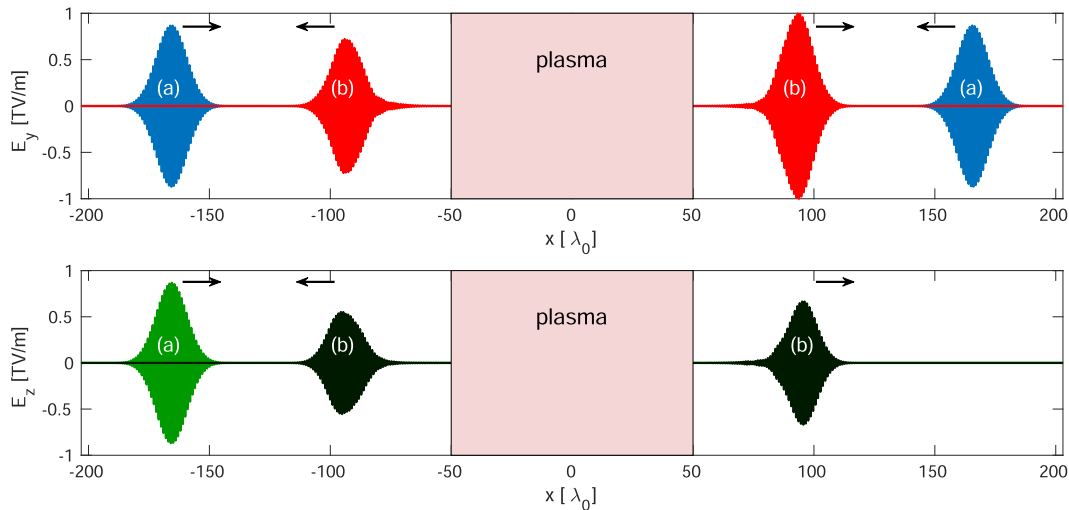


FIG. 4. Electric fields E_y and E_z at times (a) $t = 400$ fs (blue and green lines) and (b) $t = 1100$ fs (red and black lines), i.e., before (a) and after (b) the interaction inside the plasma (indicated by the central box). The arrows indicate the propagation direction of each pulse component, and the parameter values are the same as those for Fig. 2.

the pulse interaction, respectively. Because the duration of the transmitted and reflected components of E_z is almost identical to that of the incoming pulses, R and T can also be interpreted as the fractions of the power that are transmitted or reflected, respectively. Figure 5(a) shows how R and T depend on the pulse duration τ for three different values of the intensity I_0 of the driving pulses. Note that the grating length L is proportional to the pulse duration τ .

Two tendencies are evident. First, the transmission (resp. reflection) decreases (resp. increases) with increasing pulse duration τ . Second, there is a crossover point $\tau_{\text{crossover}}$ after which reflection dominates transmission, and $\tau_{\text{crossover}}$ decreases with increasing intensity I_0 .

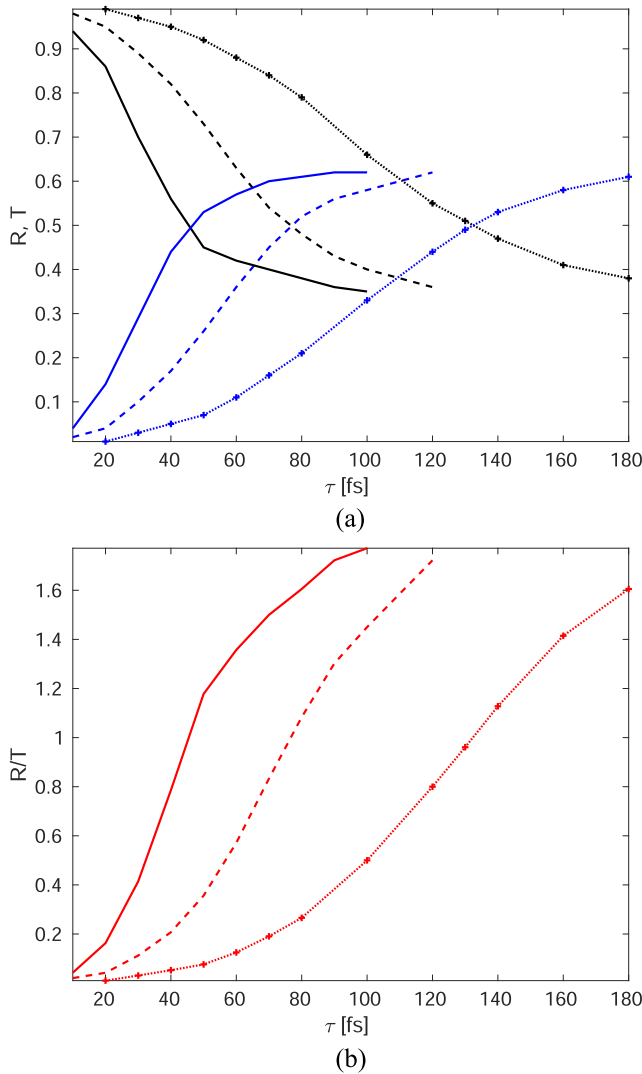


FIG. 5. (a) Transmission ratio T (black lines) and reflection ratio R (blue or light gray lines) as functions of the FWHM pulse duration τ . (b) Ratio R/T as a function of τ . The line styles in (a) and (b) correspond to the intensities 10^{17} W/cm² (solid lines), 5×10^{16} W/cm² (dashed lines), and 2.5×10^{16} W/cm² (dotted lines with crosses).

III. FOUR-WAVE-MIXING MODEL AND ITS PREDICTIONS

In this section, we discuss the interaction of the E_z pulse with an electron grating by four-wave mixing. Note that the present situation differs significantly from degenerate four-wave-mixing⁵⁵ because the latter occurs only for four parallel polarized waves.

A. Reflection and transmission in four-wave-mixing model

In the present case, the four waves are polarized in the y and z directions, and the four-wave scenario is shown schematically in Fig. 6. Waves 2 and 4 constitute a circularly (or elliptically) polarized laser pulse from the left, while wave 1 corresponds to a linearly (y -)polarized laser pulse from the right. Note that the analytical treatment is for waves and not pulses, given that the latter would require numerical evaluation of some integrals; nevertheless, the following simplified theory reproduces the main scaling behavior.

In the following, we distinguish between the y -polarized pulses 1 and 2 (also called pump waves) and the z -polarized pulse 4 that because of transmission and reflection also generates the wave-3 pulse. Via their ponderomotive forces, the two y -polarized pump waves 1 and 2 generate a density grating, and depending on the amplitudes, we are in either the collective or trapping regime.^{5,10,22,32,44,59,60} The initial (relative) electron density perturbation $\delta n_e = \frac{\Delta n_e}{n_0}$ obeys the equation

$$\delta \ddot{n}_e + \omega_{pe}^2 \delta n_e = \omega_b^2 \cos(\Psi) \quad (1)$$

with

$$\omega_{pe}^2 = \frac{4\pi n_0 e^2}{m_e}, \quad \omega_b^2 = 2|a_1 a_2| \omega_0^2, \quad \Psi = 2k_0 x, \quad (2)$$

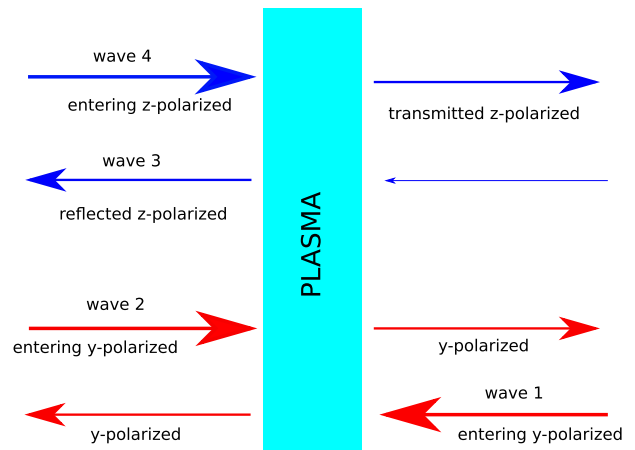


FIG. 6. Visualization of four-wave-mixing scenario discussed herein. Waves 1 and 2 produce the grating, while wave 4 propagates therein, becoming partially transmitted and partially reflected (the latter being wave 3). Shown here is a general four-wave-mixing scenario, including wave 3 in the region $L \leq x < \infty$ originating from $+\infty$; however, in the present application, the amplitude $A_3(L)$ of wave 3 at the right plasma boundary is zero.

where k_0 is the common wavenumber of waves 1 and 2 with common frequency ω_0 . The vector potential \vec{A} is normalized as $\vec{a} = \frac{e\vec{A}}{m_e c}$. Damping could be included but is neglected here for clarity.

The general solution of Eq. (1) is

$$\delta n_e(t) = \delta n_{e0} \cos(\omega_{pe}t) + \delta \dot{n}_{e0} \frac{1}{\omega_{pe}} \sin(\omega_{pe}t) + \int_0^t dt' \frac{\sin(\omega_{pe}[t-t'])}{\omega_{pe}} \omega_b^2 \cos(\Psi), \quad (3)$$

and for constant ω_b^2 we have the special inhomogeneous solution

$$\delta n_e(t) = \frac{\omega_b^2}{\omega_{pe}^2} \cos(\Psi)(1 - \cos[\omega_{pe}t]), \quad (4)$$

which will be used. As mentioned above, generalizations are straightforward. Equation (4) has two contributions: one is constant in time and is referred to as a stationary grating, and the other oscillates with frequency ω_{pe} . One might suppose that the latter would stimulate direct Raman scattering, but that is impossible because of the missing resonance in space due to the spatial mismatch originating from wavenumber $2k_0$.

For the following discussion, it is helpful to use

$$\cos \Psi \equiv \frac{e^{2ik_0x} + e^{-2ik_0x}}{2} \quad (5)$$

and

$$\cos(\omega_{pe}t) \equiv \frac{e^{i\omega_{pe}t} + e^{-i\omega_{pe}t}}{2} \quad (6)$$

when using the wave equation for waves 3 and 4, i.e.,

$$\left(c^2 \nabla^2 - \frac{\partial^2}{\partial t^2} - \omega_{pe}^2 \right) \vec{E} = \omega_{pe}^2 \delta n_e \vec{E}. \quad (7)$$

Inserting only the stationary part of Eq. (4), i.e.,

$$\delta n_e(t) = \frac{\omega_b^2}{2\omega_{pe}^2} \left(e^{2ik_0x} + e^{-2ik_0x} \right), \quad (8)$$

into Eq. (7) and collecting terms with equal phases, for the amplitudes A_3 and A_4 of the z -polarized pulses under the approximation of a slowly varying envelope, we obtain

$$2ik_0 c^2 \frac{dA_4}{dx} = \frac{\omega_b^2}{2} A_3, \quad (9)$$

$$-2ik_0 c^2 \frac{dA_3}{dx} = \frac{\omega_b^2}{2} A_4. \quad (10)$$

The four-wave-mixing model contains the laser amplitudes via the trapping frequency ω_b , so in principle the starting equations are nonlinear. However, we linearize the model by assuming constant

intensity (i.e., constant ω_b) of the lasers generating the electron grating. The laser intensities appear in the coefficient

$$\kappa = \frac{\omega_b^2}{4k_0 c^2} \quad (11)$$

when we write the general solutions as

$$A_3(x) = \alpha e^{\kappa x} + \beta e^{-\kappa x}, \quad A_4(x) = \tilde{\alpha} e^{\kappa x} + \tilde{\beta} e^{-\kappa x}. \quad (12)$$

We start with $A_3(x)$ and assume interaction in the plasma between zero and L , in which case we have

$$A_3(0) = \alpha + \beta, \quad A_3(L) = \alpha e^{\kappa L} + \beta e^{-\kappa L}, \quad (13)$$

which lead to

$$\alpha = \frac{1}{e^{-\kappa L} - e^{\kappa L}} \left[e^{-\kappa L} A_3(0) - A_3(L) \right], \quad (14)$$

$$\beta = \frac{1}{e^{-\kappa L} - e^{\kappa L}} \left[-e^{\kappa L} A_3(0) + A_3(L) \right]. \quad (15)$$

A similar calculation can be done for $\tilde{\alpha}$ and $\tilde{\beta}$ upon changing the subscript from 3 to 4.

Next, we make the natural assumption $A_3(L) = 0$ and obtain

$$\alpha = \frac{e^{-\kappa L}}{e^{-\kappa L} - e^{\kappa L}} A_3(0), \quad \beta = -\frac{e^{\kappa L}}{e^{-\kappa L} - e^{\kappa L}} A_3(0). \quad (16)$$

Considering

$$i\kappa A_4 = \frac{dA_3}{dx} = \kappa \alpha e^{\kappa x} - \kappa \beta e^{-\kappa x}, \quad (17)$$

we solve for $A_4(x)$, leading to $A_4(0)$ and $A_4(L)$ in terms of $A_3(0)$, i.e.,

$$A_4(0) = -i \frac{e^{-\kappa L} + e^{\kappa L}}{e^{-\kappa L} - e^{\kappa L}} A_3(0), \quad (18)$$

$$A_4(L) = -i \frac{2}{e^{-\kappa L} - e^{\kappa L}} A_3(0), \quad (19)$$

from which follow immediately

$$A_3(0) = i \frac{e^{-\kappa L} - e^{\kappa L}}{e^{-\kappa L} + e^{\kappa L}} A_4(0), \quad (20)$$

$$A_4(L) = \frac{2}{e^{-\kappa L} + e^{\kappa L}} A_4(0). \quad (21)$$

Thus, we have expressed the reflected amplitude $A_3(0)$ and the transmitted amplitude $A_4(L)$ in terms of the incident amplitude $A_4(0)$. Note that

$$|A_3(0)| \leq |A_4(0)| \quad \text{and} \quad |A_4(L)| \leq |A_4(0)|. \quad (22)$$

The relative strength of reflection and transmission is shown in Fig. 7(a). Unlike in the case of parallel polarization of all four waves,⁵⁵ the present device does not act as a reflection amplifier.

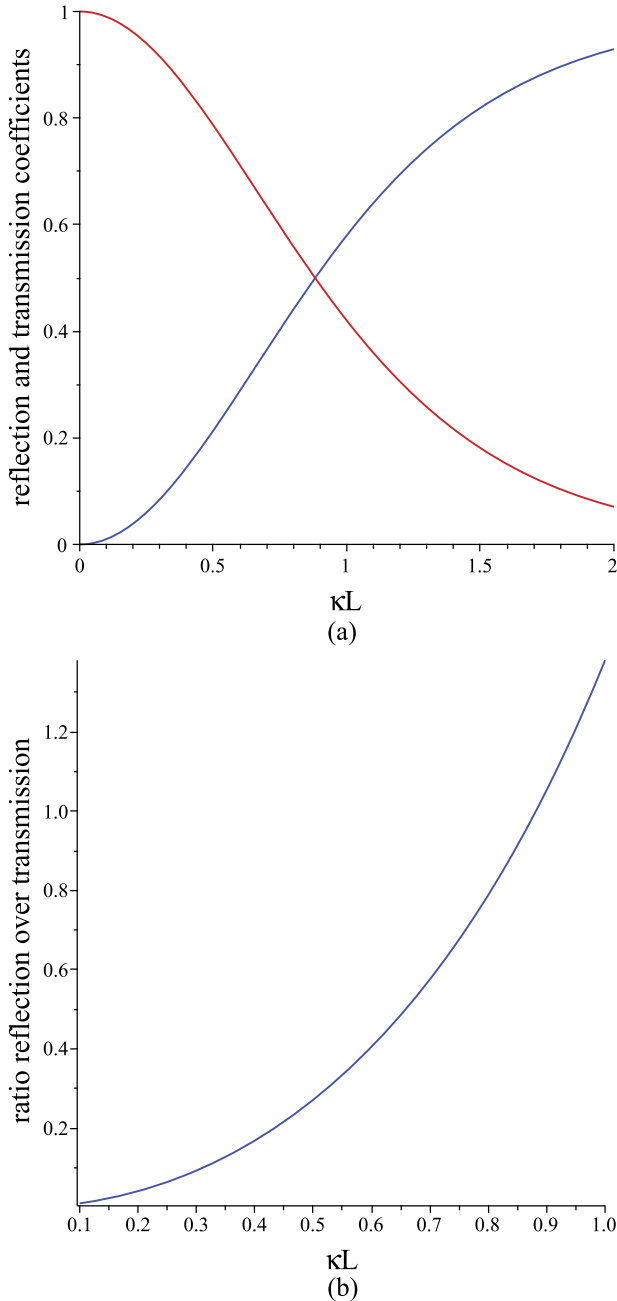


FIG. 7. (a) Plots of reflection coefficient $\mathcal{R} = \left| \frac{e^{-x} - e^x}{e^{-x} + e^x} \right|^2$ (blue) and transmission coefficient $\mathcal{T} = \left| \frac{2}{e^{-x} + e^x} \right|^2$ (red) as functions of κL . (b) Ratio \mathcal{R}/\mathcal{T} of reflection over transmission as a function of κL .

We recognize clearly the dependence on the length L of the system. Previous plasma-grating calculations were for infinite extent, but of course finite systems can be considered by a matrix approach without using Bloch's theorem, and such a calculation is presented in the Appendix.

An electron grating of infinite extent would lead to a band gap for waves with the same frequency ω as that of the pump waves (with frequency ω_0), and this agrees with the behavior shown in Fig. 7(b) for $\kappa L \rightarrow \infty$. The power reflectivity \mathcal{R} and the power transmission \mathcal{T} are defined as

$$\mathcal{R} = \frac{|A_3(0)|^2}{|A_4(0)|^2} \quad \text{and} \quad \mathcal{T} = \frac{|A_3(L)|^2}{|A_4(0)|^2} \quad (23)$$

and are readily identified with R and T , respectively, as obtained from the simulation results in Fig. 5. Note that $\mathcal{R} + \mathcal{T} = 1$ holds.

The factor i in $A_3(0)$ points to a phase change of the backward-propagating E_z wave. However, because we consider only a one-dimensional configuration, we cannot draw conclusions about phase conjugation.

B. Parameter κL

Although simplified considerably, the present model should explain the scaling behavior seen in the numerical results. Specifically, the pump-amplitude dependence and the finite-length effects are contained in the dependencies on the parameter κL .

First, for fixed intensity I_0 (i.e., fixed κ), the theory predicts that \mathcal{R}/\mathcal{T} increases with L [Fig. 7(b)], and this is exactly what the simulations showed [Fig. 5(b)]. Second, the theory predicts that for smaller intensity I_0 (i.e., smaller κ) we obtain a crossover from transmission-dominated to reflection-dominated conditions at larger L [Fig. 7(a)], and because L corresponds directly to τ , this again explains the simulation results in Fig. 5.

Most of the present PIC simulations were performed for $\kappa L \sim \mathcal{O}(1)$. For example, for pulses with power intensity $I_0 = 5 \times 10^{16} \text{ W/cm}^2$, we have $a_0^2 \approx 2.3 \times 10^{-2}$ and $\omega_b \approx 0.21\omega_0$, which we evaluate for $\omega_0 \approx 2.4 \times 10^{15} \text{ s}^{-1}$. For laser pulses of 40 fs in duration, we estimate L from $\frac{L}{c} \approx 40 \text{ fs}$ and obtain $\kappa L \approx 1.1$. For such a value, according to Fig. 7, reflection of E_z will be of the same order, which agrees remarkably well with the PIC simulations.

IV. SUMMARY AND DISCUSSION

Herein, we studied a dynamic electron grating driven by counter-propagating lasers. The fast electron response also occurs during the initial development of an ion grating, but in the case of short pump pulses it is the only significant plasma reaction. The lifetime of a pure electron grating is short (depending on the pump-pulse duration and the inverse ion plasma frequency), and the structure develops rapidly and may be of interest for studying frequency conversion. Also, a pure electron grating is of finite extent, and so infinite-length theories based on Bloch wave solutions are inappropriate for investigating the optical properties of an electron grating.

The specific scenario studied herein—i.e., the z component of a circularly polarized pulse experiencing an electron grating driven by the y components of that pulse and a second linearly polarized

pulse—can be interpreted as either an ultra-fast pulse splitter (in reflection and transmission) or a mechanism for altering the polarization state of the circularly polarized laser pulse.

To investigate interaction with other waves, it is important to take due note of the finite lifetime. We overcame this difficulty by preparing a specific initial configuration: one of the pump laser pulses was linearly (y -)polarized, while the other had circular polarization, and we decomposed the latter into the y and z directions. The interaction of the y components led to the development of a steady electron grating, and the z component felt the density ripples and was partially reflected and partially transmitted. The ratio of reflection to transmission depended on several parameters, and we considered in detail the sensitivity to the pulse strength and duration. One-dimensional PIC simulations supplied data over a broad range, and the theoretical interpretation via four-wave mixing showed the dependence on κL that correctly described the numerical findings.

In some respects, the present modeling perhaps oversimplifies what is actually a complex situation. Another scheme that could be used to analyze the present configuration is outlined in the [Appendix](#). The finite transfer-matrix method may be applied and generalized to handle different aspects such as inhomogeneity and random variations in the height and strength of the unit cells, but we leave that for future considerations (also for other types of gratings). Currently, the four-wave-mixing theory is sufficient for a rough classification of the main phenomena.

In the present work, we studied the possibility of using electron gratings as pulse splitters, but the range of possible applications seems much wider, and it seems reasonable to expect that many of the previously investigated applications of ion gratings (e.g., wave plates, polarizers, holograms) could also be realized with fast electron gratings. Further work is in progress, especially on the transition from a short electron grating to a wider (more extended) ion grating. In asymmetric situations (i.e., when gratings are produced by pulses of different lengths), density modulations and wake fields may act as seeds for effective Raman scattering. Returning to the present configuration, we reason that frequency up-conversion in a rapidly developing electron grating requires further attention, with the potential to give new insights into basic phenomena.

ACKNOWLEDGMENTS

Computational support and infrastructure were provided by the Centre for Information and Media Technology (ZIM) at the University of Düsseldorf (Germany). Development of the EPOCH PIC code used in this work was funded in part by the Engineering and Physical Sciences Research Council (UK) (Grant Nos. EP/G054950/1, EP/G056803/1, EP/G055165/1, and EP/M022463/1).

AUTHOR DECLARATIONS

Conflict of Interest

The authors have no conflicts to disclose.

Author Contributions

G. Lehmann: Conceptualization (equal); Formal analysis (equal); Investigation (equal); Methodology (equal); Writing – original draft

(equal); Writing – review & editing (equal). **K. H. Spatschek:** Conceptualization (equal); Formal analysis (equal); Investigation (equal); Methodology (equal); Writing – original draft (equal); Writing – review & editing (equal).

DATA AVAILABILITY

The data that support the findings of this study are available from the corresponding author upon reasonable request.

APPENDIX: REFLECTION AND TRANSMISSION BY TRANSFER-MATRIX METHOD

To investigate the properties of a finite electron grating, one may also use the transfer-matrix method for periodic structures.⁶¹ In that description, one starts from simple variations of the dielectric constant, as done in Refs. 10 and 52 for example. However, unlike for an ion grating, for an electron grating we cannot apply the Bloch wave solution of the Maxwell equations⁶² because an electron grating is finite in extent.

Here, we split the whole grating (within the block named “plasma” in [Fig. 6](#)) into N unit cells of length $\Lambda = a + b$, where we have refractive index n_1 over distance a and refractive index n_2 over distance b . The transverse electric field component $E_z \equiv E$ (note that for simplicity, we omit the index z in this Appendix) is a function of x , and we write it as

$$E(x) = c_m e^{-ik_{2z}(x-m\Lambda+a)} + d_m e^{+ik_{2z}(x-m\Lambda+a)} \quad (\text{A1})$$

for $(m-1)\Lambda < x < m\Lambda - a$, where $m = 1, 2, \dots, N$. Similarly, we write

$$E(x) = a_m e^{-ik_{2z}(x-m\Lambda)} + d_m e^{+ik_{2z}(x-m\Lambda)} \quad (\text{A2})$$

for $m\Lambda - a < x < m\Lambda$. Following Yeh,⁶¹ we obtain

$$\begin{pmatrix} a_m \\ b_m \end{pmatrix} = \begin{pmatrix} D & -B \\ -C & A \end{pmatrix}^m \begin{pmatrix} a_0 \\ b_0 \end{pmatrix} \equiv T^m \begin{pmatrix} a_0 \\ b_0 \end{pmatrix}, \quad (\text{A3})$$

where for TE waves we have

$$A = e^{ik_1 a} \left[\cos(k_2 b) + \frac{i}{2} \left(\frac{k_2}{k_1} + \frac{k_1}{k_2} \right) \sin(k_2 b) \right], \quad (\text{A4})$$

$$B = e^{-ik_1 a} \frac{i}{2} \left(\frac{k_2}{k_1} - \frac{k_1}{k_2} \right) \sin(k_2 b), \quad (\text{A5})$$

$$C = -e^{ik_1 a} \frac{i}{2} \left(\frac{k_2}{k_1} - \frac{k_1}{k_2} \right) \sin(k_2 b), \quad (\text{A6})$$

$$D = e^{-ik_1 a} \left[\cos(k_2 b) - \frac{i}{2} \left(\frac{k_2}{k_1} + \frac{k_1}{k_2} \right) \sin(k_2 b) \right]. \quad (\text{A7})$$

We abbreviate as $T^m \equiv T_m$. The wavenumbers $k_{1,2}$ are in the x direction with magnitudes $k_{1,2} = n_{1,2} \frac{\omega_0}{c}$. The refractive indices n_1 and n_2 follow from the particle densities n_a and n_b in regions a and b , respectively. Denoting the plasma frequencies in regions a and b by ω_{pea} and ω_{peb} , respectively, we have

$$n_{1,2} = \sqrt{1 - \frac{\omega_{pea,b}^2}{\omega^2}}. \quad (\text{A8})$$

The coefficients A , B , C , and D satisfy

$$AD - BC = 1 \quad \text{or} \quad (A - D)^2 + 4BC = (A + D)^2 - 4. \quad (\text{A9})$$

It is straightforward to show that the transfer matrix

$$T_N \equiv \begin{pmatrix} T_{11} & T_{12} \\ T_{21} & T_{22} \end{pmatrix} \quad (\text{A10})$$

is related to the scattering matrix (S-matrix) via

$$S \equiv \begin{pmatrix} r & \tilde{t} \\ t & \tilde{r} \end{pmatrix} = \begin{pmatrix} -\frac{T_{12}}{T_{11}} & \frac{1}{T_{11}} \\ \frac{1}{T_{11}} & \frac{T_{21}}{T_{11}} \end{pmatrix}. \quad (\text{A11})$$

The reflection rate $\mathcal{R} = |r|^2$, the transmission rate $\mathcal{T} = |t|^2$, and the reflection-to-transmission ratio $\rho = \frac{\mathcal{R}}{\mathcal{T}}$ follow from

$$\mathcal{R} = \left| \frac{T_{12}}{T_{11}} \right|^2, \quad \mathcal{T} = \left| \frac{1}{T_{11}} \right|^2, \quad \rho = |T_{12}|^2. \quad (\text{A12})$$

We determine the entries $T_{\mu\nu}$ ($\mu, \nu = 1, 2$) by diagonalizing T , i.e.,

$$T_{\text{diag}}^{-1} T T_{\text{diag}} = \begin{pmatrix} \lambda_+ & 0 \\ 0 & \lambda_- \end{pmatrix} \quad \text{for} \quad T = \begin{pmatrix} D & -B \\ -C & A \end{pmatrix}, \quad (\text{A13})$$

where the eigenvalues of T are

$$\lambda_{\pm} = \frac{1}{2}(A + D) \pm \frac{1}{2}\sqrt{(A + D)^2 - 4}. \quad (\text{A14})$$

We introduce the abbreviation

$$W \equiv \sqrt{(A + D)^2 - 4} \quad (\text{A15})$$

and find T_{diag} from the eigenvectors, i.e.,

$$T_{\text{diag}} = \begin{pmatrix} \frac{2B}{-A + D - W} & \frac{2B}{-A + D + W} \\ 1 & 1 \end{pmatrix}. \quad (\text{A16})$$

The inverse is

$$T_{\text{diag}}^{-1} = \frac{1}{W} \begin{pmatrix} -C & \frac{1}{2}(A - D + W) \\ C & \frac{1}{2}(-A + D + W) \end{pmatrix}. \quad (\text{A17})$$

The diagonalization process leads to

$$\begin{pmatrix} T_{11} & T_{12} \\ T_{21} & T_{22} \end{pmatrix} = T_{\text{diag}} \begin{pmatrix} \lambda_+^N & 0 \\ 0 & \lambda_-^N \end{pmatrix} T_{\text{diag}}^{-1}, \quad (\text{A18})$$

from which transmission and reflection can be determined in the case of N unit cells.

To determine the transmission rate, we require the element T_{11} , and we find

$$T_{11} = \frac{AD - 1}{W} \left[\frac{A + D + W}{A - D + W} \lambda_+^{N-1} - \frac{A + D - W}{A - D - W} \lambda_-^{N-1} \right] \rightsquigarrow \mathcal{T} = \frac{1}{|T_{11}|^2}. \quad (\text{A19})$$

From the definition (A14), we recognize that $A + D$ plays the leading role. For

$$|A + D| \geq 2 \quad \rightsquigarrow \quad T_{\text{transition}} \rightarrow 0 \quad \text{for} \quad N \rightarrow \infty, \quad (\text{A20})$$

because either $|\lambda_+|$ or $|\lambda_-|$ will be greater than 1.

The element T_{12} determines the ratio of reflection to transmission, i.e.,

$$T_{12} = \frac{B}{W} (\lambda_-^N - \lambda_+^N) \quad \rightsquigarrow \quad \rho \equiv \frac{\mathcal{R}}{\mathcal{T}} = |T_{12}|^2. \quad (\text{A21})$$

On one hand, for

$$|A + D| \geq 2 \quad \rightsquigarrow \quad \rho \rightarrow \infty \quad \text{for} \quad N \rightarrow \infty. \quad (\text{A22})$$

On the other hand, for

$$|A + D| < 2 \quad \rightsquigarrow \quad |\lambda_{\pm}| = 1 \quad \rightsquigarrow \quad \rho = 0. \quad (\text{A23})$$

Wave propagation with corresponding wavenumber k and frequency ω will be possible.

The numerical evaluation requires specification of n_0/n_c , n_1 , n_2 , a , b , ω , and N . Figure 8 shows an evaluation of $\rho \equiv \frac{\mathcal{R}}{\mathcal{T}} = |T_{12}|^2$ as a function of the number N of unit cells. The parameter values are $\frac{n_0}{n_c} = 0.05$, $\frac{a}{\Lambda} = \frac{b}{\Lambda} = 0.5$, $\frac{n_a}{n_0} = 1.8$ and $\frac{n_b}{n_0} = 0.2$, and the frequency is $\omega = \omega_0$. Bloch wave calculations for an infinite system (corresponding to $N \rightarrow \infty$) would show a band gap for this frequency (corresponding to $|T_{12}|^2 \rightarrow \infty$), and indeed we see that this behavior is realized for $N \rightarrow \infty$. However, substantial transmission becomes possible for smaller N , and so we understand the partial transparency of the finite electron grating for the E_z component of the incident pulse.

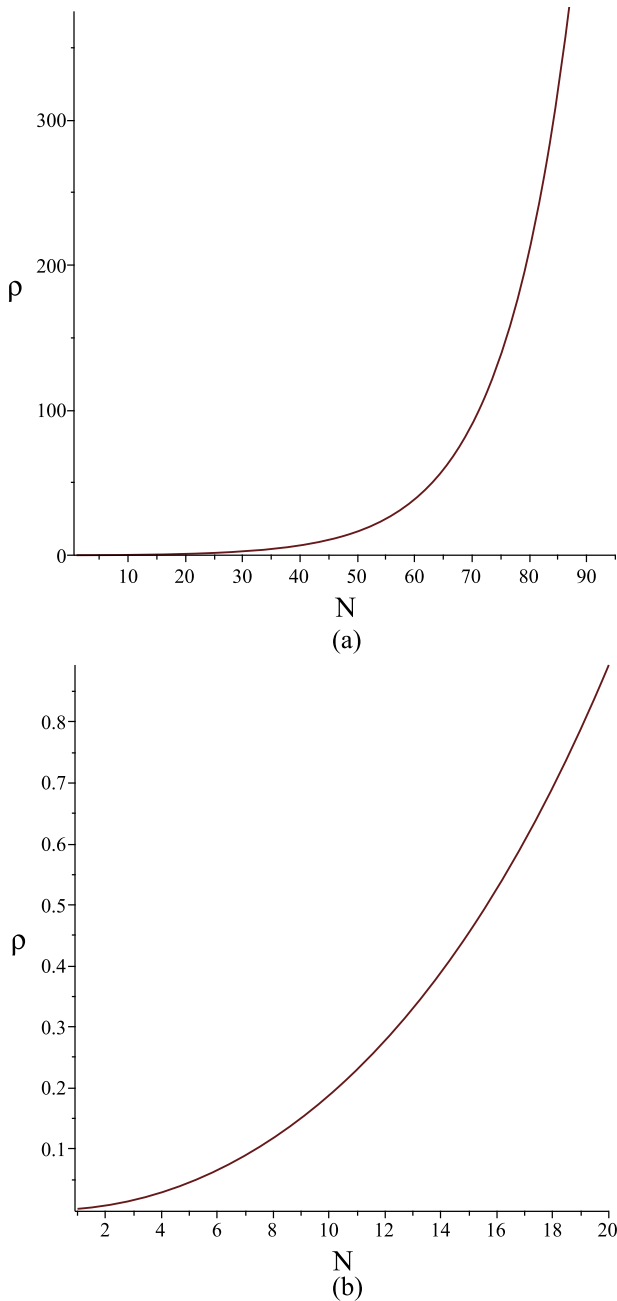


FIG. 8. Plot of $\rho \equiv \mathcal{R}/\mathcal{T} = |T_{12}|^2$ vs N for $n_0 = 0.05n_c$, $a = b = 0.5\Lambda$, $n_a = 1.8n_0$, and $n_b = 0.2n_0$. The frequency is $\omega = \omega_0$. Subfigure (a) shows that for $N \rightarrow \infty$, the bangap of an infinite configuration is obtained. Subfigure (b) is a magnified part of subfigure (a) for better comparison with the numerical results.

However, a grating produced by short pump pulses will show spatial inhomogeneity, so the strict assumption of periodicity is not satisfied. In future work, we will account for the spatial inhomogeneity and randomness of gratings, in which case the present finite transfer-matrix method may be the method of choice.

The Bloch wave case (infinite grating) occurs for $N \rightarrow \infty$, and in the case of strict periodicity we find

$$e^{\pm iK\Lambda} \triangleq \lambda_{\pm}, \quad (\text{A24})$$

where K is the Bloch wavenumber. The band structure and condition for transmission follow from⁵⁵

$$K = \frac{1}{\Lambda} \arccos \left[\frac{1}{2}(A + D) \right]. \quad (\text{A25})$$

Note here the correspondence to the previous discussion of the magnitude of $A + D$. The infinite situation with $N \rightarrow \infty$ predicts band gaps, whereas a theory for finite N results in a finite ratio ρ , and for $|A + D| < 2$ we find propagating modes.

REFERENCES

- ¹V. M. Malkin and N. J. Fisch, "Manipulating ultraintense laser pulses in plasmas," *Phys. Plasmas* **12**, 044507 (2005).
- ²H. Peng, J.-R. Marquès, L. Lancia, F. Amiranoff, R. L. Berger, S. Weber, and C. Riconda, "Plasma optics in the context of high intensity lasers," *Matter Radiat. Extremes* **4**, 065401 (2019).
- ³P. Michel, "Plasma photonics: Manipulating light using plasmas," Technical Report No. 818220, Lawrence Livermore National Laboratory, 2021, <https://www.osti.gov/servlets/purl/1756740>.
- ⁴S. Monchocé, S. Kahaly, A. Leblanc, L. Videau, P. Combis, F. Réau, D. Garzella, P. D'Oliveira, P. Martin, and F. Quéré, "Optically controlled solid-density transient plasma gratings," *Phys. Rev. Lett.* **112**, 145008 (2014).
- ⁵G. Lehmann and K. H. Spatschek, "Laser-driven plasma photonic crystals for high-power lasers," *Phys. Plasmas* **24**, 056701 (2017).
- ⁶D. Turnbull, P. Michel, T. Chapman, E. Tubman, B. B. Pollock, C. Y. Chen, C. Goyon, J. S. Ross, L. Divol, N. Woolsey, and J. D. Moody, "High power dynamic polarization control using plasma photonics," *Phys. Rev. Lett.* **116**, 205001 (2016).
- ⁷K. Qu, Q. Jia, and N. J. Fisch, "Plasma q-plate for generation and manipulation of intense optical vortices," *Phys. Rev. E* **96**, 053207 (2017).
- ⁸D. J. Stark, C. Bhattacharjee, A. V. Arefiev, T. Toncian, R. D. Hazeltine, and S. M. Mahajan, "Relativistic plasma polarizer: Impact of temperature anisotropy on relativistic transparency," *Phys. Rev. Lett.* **115**, 025002 (2015).
- ⁹D. Turnbull, C. Goyon, G. E. Kemp, B. B. Pollock, D. Mariscal, L. Divol, J. S. Ross, S. Patankar, J. D. Moody, and P. Michel, "Refractive index seen by a probe beam interacting with a laser-plasma system," *Phys. Rev. Lett.* **118**, 015001 (2017).
- ¹⁰G. Lehmann and K. H. Spatschek, "Plasma-based polarizer and waveplate at large laser intensity," *Phys. Rev. E* **97**, 063201 (2018).
- ¹¹L. L. Yu, Y. Zhao, L. J. Qian, M. Chen, S. M. Weng, Z. M. Sheng, D. A. Jaroszynski, W. B. Mori, and J. Zhang, "Plasma optical modulators for intense lasers," *Nat. Commun.* **7**, 11893 (2016).
- ¹²R. Pompili, M. P. Anania, M. Bellaveglia, A. Biagioni, S. Bini, F. Bisesto, E. Brentegani, F. Cardelli, G. Castorina, E. Chiadroni, A. Cianchi, O. Coiro, G. Costa, M. Croia, D. Di Giovenale, M. Ferrario, F. Filippi, A. Giribono, V. Lollo, A. Marocchino, M. Marongiu, V. Martinelli, A. Mostacci, D. Pellegrini, L. Piersanti, G. Di Pirro, S. Romeo, A. R. Rossi, J. Scifo, V. Shpakov, A. Stella, C. Vaccarezza, F. Villa, and A. Zigler, "Focusing of high-brightness electron beams with active-plasma lenses," *Phys. Rev. Lett.* **121**, 174801 (2018).
- ¹³C. A. Lindström, E. Adli, G. Boyle, R. Corsini, A. E. Dyson, W. Farabolini, S. M. Hooker, M. Meisel, J. Osterhoff, J.-H. Röckemann, L. Schaper, and K. N. Sjobak, "Emittance preservation in an aberration-free active plasma lens," *Phys. Rev. Lett.* **121**, 194801 (2018).
- ¹⁴M. Nakatsutsumi, A. Kon, S. Buffechoux, P. Audebert, J. Fuchs, and R. Kodama, "Fast focusing of short-pulse lasers by innovative plasma optics toward extreme intensity," *Opt. Lett.* **35**, 2314 (2010).

- ¹⁵M. Zeng, A. Martinez de la Ossa, K. Poder, and J. Osterhoff, "Plasma lenses for relativistic laser beams in laser wakefield accelerators," *Phys. Plasmas* **27**, 023109 (2020).
- ¹⁶I. Y. Dodin and N. J. Fisch, "Storing, retrieving, and preprocess optical information by Raman backscattering in plasmas," *Phys. Rev. Lett.* **88**, 165001 (2002).
- ¹⁷I. Y. Dodin and N. J. Fisch, "Dynamic volume holography and optical information processing by Raman scattering," *Opt. Commun.* **214**, 83–98 (2002).
- ¹⁸G. Lehmann and K. H. Spatschek, "Plasma volume holograms for focusing and mode conversion of ultraintense laser pulses," *Phys. Rev. E* **100**, 033205 (2019).
- ¹⁹M. R. Edwards, V. R. Munirov, A. Singh, N. M. Fasano, E. Kur, N. Lemos, J. M. Mikhailova, J. S. Wurtele, and P. Michel, "Holographic plasma lenses," *Phys. Rev. Lett.* **128**, 065003 (2022).
- ²⁰G. Lehmann and K. H. Spatschek, "Wakefield stimulated terahertz radiation from a plasma grating," *Plasma Phys. Controlled Fusion* **64**, 034001 (2022).
- ²¹R. K. Kirkwood, D. P. Turnbull, T. Chapman, S. C. Wilks, M. D. Rosen, R. A. London, L. A. Pickworth, W. H. Dunlop, J. D. Moody, D. J. Strozzi, P. A. Michel, L. Divol, O. L. Landen, B. J. MacGowan, B. M. Van Woutherghem, K. B. Fournier, and B. E. Blue, "Plasma-based beam combiner for very high fluence and energy," *Nat. Phys.* **14**, 80 (2017).
- ²²G. Shvets, N. J. Fisch, A. Pukhov, and J. Meyer-ter-Vehn, "Superradiant amplification of an ultrashort laser pulse in a plasma by a counterpropagating pump," *Phys. Rev. Lett.* **81**, 4879 (1998).
- ²³V. M. Malkin, G. Shvets, and N. J. Fisch, "Fast compression of laser beams to highly overcritical powers," *Phys. Rev. Lett.* **82**, 4448–4451 (1999).
- ²⁴L. Lancia, A. Giribono, L. Vassura, M. Chiaramello, C. Riconda, S. Weber, A. Castan, A. Chatelain, A. Frank, T. Gangolf, M. N. Quinn, J. Fuchs, and J. R. Marquès, "Signatures of the self-similar regime of strongly coupled stimulated Brillouin scattering for efficient short laser pulse amplification," *Phys. Rev. Lett.* **116**, 075001 (2016).
- ²⁵A. E. Hussein, J. Ludwig, K. Behm, Y. Horovitz, P.-E. Masson-Laborde, V. Chvykov, A. Maksimchuk, T. Matsuoka, C. McGuffey, V. Yanovsky, W. Rozmus, and K. Krushelnick, "Stimulated Raman backscattering from a laser wakefield accelerator," *New J. Phys.* **20**, 073039 (2018).
- ²⁶J.-R. Marquès, L. Lancia, T. Gangolf, M. Blecher, S. Bolanos, J. Fuchs, O. Willi, F. Amiranoff, R. L. Berger, M. Chiaramello, S. Weber, and C. Riconda, "Joule-level high-efficiency energy transfer to sub-picosecond laser pulses by a plasma-based amplifier," *Phys. Rev. X* **9**, 021008 (2019).
- ²⁷Z. Wu, Q. Chen, A. Morozov, and S. Suckewer, "Compression of laser pulses by near-forward Raman amplification in plasma," *Phys. Plasmas* **27**, 013104 (2020).
- ²⁸A. Frank, J. Fuchs, L. Lancia, G. Lehmann, J.-R. Marquès, G. Mourou, C. Riconda, K. H. Spatschek, T. Toncian, L. Vassura, S. Weber, and O. Willi, "Amplification of ultra-short light pulses by ion collective modes in plasmas," *Eur. Phys. J.: Spec. Top.* **223**, 1153–1156 (2014).
- ²⁹Z.-M. Sheng, J. Zhang, and D. Umstadter, "Plasma density gratings induced by intersecting laser pulses in underdense plasmas," *Appl. Phys. B* **77**, 673 (2003).
- ³⁰P. Michel, L. Divol, E. A. Williams, S. Weber, C. A. Thomas, D. A. Callahan, S. W. Haan, J. D. Salmonson, S. Dixit, D. E. Hinkel, M. J. Edwards, B. J. MacGowan, J. D. Lindl, S. H. Glenzer, and L. J. Suter, "Tuning the implosion symmetry of ICF targets via controlled crossed-beam energy transfer," *Phys. Rev. Lett.* **102**, 025004 (2009).
- ³¹P. Michel, L. Divol, D. Turnbull, and J. D. Moody, "Dynamic control of the polarization of intense laser beams via optical wave mixing in plasmas," *Phys. Rev. Lett.* **113**, 205001 (2014).
- ³²G. Lehmann and K. H. Spatschek, "Transient plasma photonic crystal for high-power lasers," *Phys. Rev. Lett.* **116**, 225002 (2016).
- ³³H. Peng, C. Riconda, M. Grech, J. Q. Su, and S. Weber, "Nonlinear dynamics of laser-generated ion-plasma gratings: A unified description," *Phys. Rev. E* **100**, 061201 (2019).
- ³⁴S. E. Schrauth, A. Colaitis, R. L. Luthi, R. C. W. Plummer, W. G. Hollingsworth, C. W. Carr, M. A. Norton, R. J. Wallace, A. V. Hamza, B. J. MacGowan, M. J. Shaw, M. L. Spaeth, K. R. Manes, P. Michel, and J.-M. Di Nicola, "Study of self-diffraction from laser generated plasma gratings in the nanosecond regime," *Phys. Plasmas* **26**, 073108 (2019).
- ³⁵H. Peng, C. Riconda, M. Grech, C.-T. Zhou, and S. Weber, "Dynamical aspects of plasma gratings driven by a static ponderomotive potential," *Plasma Phys. Controlled Fusion* **62**, 115015 (2020).
- ³⁶A. V. Andreev, A. V. Balakin, I. A. Ozheredov, A. P. Shkurinov, P. Masselin, G. Mouret, and D. Boucher, "Compression of femtosecond laser pulses in thin one-dimensional photonic crystals," *Phys. Rev. E* **63**, 016602 (2000).
- ³⁷H.-C. Wu, Z.-M. Sheng, Q.-J. Zhang, Y. Cang, and J. Zhang, "Controlling ultrashort intense laser pulses by plasma Bragg gratings with ultrahigh damage threshold," *Laser Part. Beams* **23**, 417–421 (2005).
- ³⁸S. Suntsov, D. Abdollahpour, D. G. Papazoglou, and S. Tzortzakos, "Femtosecond laser induced plasma diffraction gratings in air as photonic devices for high intensity laser applications," *Appl. Phys. Lett.* **94**, 251104 (2009).
- ³⁹H. Y. Chen, Y. Yin, C. L. Tian, H. Xu, Y. Y. Ma, H. B. Zhuo, and F. Q. Shao, "Moving electron density gratings induced in the beat-wave field of two counterpropagating laser pulses," *Phys. Plasmas* **17**, 083112 (2010).
- ⁴⁰S. Hocquet, J. Néauport, and N. Bonod, "Recent progress in the development of pulse compression gratings," *EPJ Web Conf.* **59**, 07002 (2013).
- ⁴¹A. Jarnak, M. Durand, A. Houard, Y. Liu, B. Prade, M. Richardson, and A. Mysyrowicz, "Spatiotemporal cleaning of a femtosecond laser pulse through interaction with counterpropagating filaments in air," *Phys. Rev. A* **89**, 023844 (2014).
- ⁴²Q. Jia, I. Barth, M. R. Edwards, J. M. Mikhailova, and N. J. Fisch, "Distinguishing Raman from strongly coupled Brillouin amplification for short pulses," *Phys. Plasmas* **23**, 053118 (2016).
- ⁴³Y. Shi, J. Vieira, R. M. G. M. Trines, R. Bingham, B. F. Shen, and R. J. Kingham, "Magnetic field generation in plasma waves driven by copropagating intense twisted lasers," *Phys. Rev. Lett.* **121**, 145002 (2018).
- ⁴⁴G. Lehmann and K. H. Spatschek, "Plasma photonic crystal growth in the trapping regime," *Phys. Plasmas* **26**, 013106 (2019).
- ⁴⁵J. R. Smith, C. Orban, G. K. Ngirmang, J. T. Morrison, K. M. George, E. A. Chowdhury, and W. M. Roquemore, "Particle-in-cell simulations of density peak formation and ion heating from short pulse laser-driven ponderomotive steepening," *Phys. Plasmas* **26**, 123103 (2019).
- ⁴⁶H. H. Ma, S. M. Weng, P. Li, X. F. Li, Y. X. Wang, S. H. Yew, M. Chen, P. Mckenna, and Z. M. Sheng, "Growth, saturation and breaking down of laser-driven plasma density gratings," *Phys. Plasmas* **27**, 073105 (2020).
- ⁴⁷F. R. Morgenthaler, "Velocity modulation of electromagnetic waves," *IEEE Trans. Microwave Theory Tech.* **6**, 167 (1958).
- ⁴⁸S. C. Wilks, J. M. Dawson, and W. B. Mori, "Frequency up-conversion of electromagnetic radiation with use of an overdense plasma," *Phys. Rev. Lett.* **61**, 337 (1988).
- ⁴⁹J. T. Mendonça and P. K. Shukla, "Time refraction and time reflection: Two basic concepts," *Phys. Scr.* **65**, 160 (2002).
- ⁵⁰K. Qu, Q. Jia, M. R. Edwards, and N. J. Fisch, "Theory of electromagnetic wave frequency upconversion in dynamic media," *Phys. Rev. E* **98**, 023202 (2018).
- ⁵¹D. Turnbull, P. Franke, J. Katz, J. P. Palastro, I. A. Begishev, R. Boni, J. Bromage, A. L. Milder, J. L. Shaw, and D. H. Froula, "Ionization waves of arbitrary velocity," *Phys. Rev. Lett.* **120**, 225001 (2018).
- ⁵²H. Peng, C. Riconda, S. Weber, C. T. Zhou, and S. C. Ruan, "Frequency conversion of lasers in a dynamic plasma grating," *Phys. Rev. Appl.* **15**, 054053 (2021).
- ⁵³E. Kur, M. Lazarow, J. S. Wurtele, and P. Michel, "Nonlinear polarization transfer and control of two laser beams overlapping in a uniform nonlinear medium," *Opt. Express* **29**, 1162 (2021).
- ⁵⁴K. B. Kwon, T. Kang, H. S. Song, Y.-K. Kim, B. Ersfeld, D. A. Jaroszynski, and M. S. Hur, "High-energy, short-duration bursts of coherent terahertz radiation from an embedded plasma dipole," *Sci. Rep.* **8**, 145 (2018).
- ⁵⁵A. Yariv and D. M. Pepper, "Amplified reflection, phase conjugation, and oscillation in degenerate four-wave mixing," *Opt. Lett.* **1**, 16 (1977).
- ⁵⁶G. P. Gupta and B. K. Sinha, "Phase conjugation in the low reflectivity regime by nearly degenerate four-wave mixing in a homogeneous plasma," *Phys. Plasmas* **5**, 2252 (1998).

⁵⁷C. Goyon, M. R. Edwards, T. Chapman, L. Divol, N. Lemos, G. J. Williams, D. A. Mariscal, D. Turnbull, A. M. Hansen, and P. Michel, “Slow and fast light in plasma using optical wave mixing,” *Phys. Rev. Lett.* **126**, 205001 (2021).

⁵⁸T. D. Arber, K. Bennett, C. S. Brady, A. Lawrence-Douglas, M. G. Ramsay, N. J. Sircombe, P. Gillies, R. G. Evans, H. Schmitz, A. R. Bell, and C. P. Ridgers, “Contemporary particle-in-cell approach to laser-plasma modelling,” *Plasma Phys. Controlled Fusion* **57**, 113001 (2015).

⁵⁹R. H. Dicke, “Coherence in spontaneous radiation processes,” *Phys. Rev.* **93**, 99 (1954).

⁶⁰M. Dreher, E. Takahashi, J. Meyer-ter-Vehn, and K. J. Witte, “Observation of superradiant amplification of ultrashort laser pulses in a plasma,” *Phys. Rev. Lett.* **93**, 095001 (2004).

⁶¹P. Yeh, *Optical Waves in Layered Media* (Wiley Interscience, New York, 1988).

⁶²Z. Zhang and S. Satpathy, “Electromagnetic wave propagation in periodic structures: Bloch wave solution of Maxwell equations,” *Phys. Rev. Lett.* **65**, 2650 (1990).